Acta Geotechnica
https://doi.org/10.1007/s11440-026-03112-4

RESEARCH PAPER

Robotic automated specimen preparation (RASP): applied to air pluviation

L. Mugele[1] · J. D. Arroyo Lopez[1] · J. Zürn[1] · H. H. Stutz[1]

Received: 29 July 2025 / Accepted: 9 May 2026

Abstract

A fully Robotic Automated Specimen Preparation (RASP) approach is introduced for granular soils using the single-nozzle dry air pluviation method. For this purpose, a nozzle is installed at the tool end of a 6-axis collaborative robot (cobot). Over 80 specimens were automatically prepared using two different granular materials and analyzed via local density measurements. Additionally, manually prepared specimens were generated for comparison. More than 1000 local density measurements have been conducted. The results demonstrate that the proposed RASP method enables a reproducible and homogeneous preparation of sand specimens, with density variations significantly lower than those observed in manually prepared specimens. The RASP enables a detailed analysis of specific preparation-influencing factors such as pluviation pattern, fall height, nozzle diameter, and nozzle velocity. In addition to the improved quality of the sand specimen preparation, the proposed RASP technique will increase efficiency and reduce economic costs in soil mechanical laboratories in the near future. Besides, the data obtained during the specimen preparation enables a data-based documentation and quality assurance of the entire preparation process.

Keywords Air pluviation · Automation · Reproducibility · Robotic · Sand specimen preparation

List of symbols

d_n	Nozzle diameter
$\dot{m}$	Mass flow rate through the nozzle
$\rho_\mathrm{d,t}$	Target density
ρ_d	Achieved density
ρ_s	Grain density
h_f	Fall height
Δh	Layer thickness
Δt	Time per layer
$v_\mathrm{n} = \lvert \boldsymbol{v}_\mathrm{n} \rvert$	Norm of the nozzle velocity
$a_\mathrm{n} = \lvert \boldsymbol{a}_\mathrm{n} \rvert$	Norm of the nozzle acceleration
D	Specimen diameter
H	Specimen height
h_r	Height of the PVC rings
l_s	Path spacing
l_x	Arc transition
α	Layer rotation angle
d_{50}	Mean grain size
d_g	Grain diameter
I_D	Relative density
$\bar{\square}$	Mean value
s	Standard deviation
CV	Coefficient of variation

✉ H. H. Stutz
hans.stutz@kit.edu

L. Mugele
luis.mugele@kit.edu

J. D. Arroyo Lopez
juan.lopez@student.kit.edu

J. Zürn
jochen.zuern@kit.edu

[1] Institute of Soil Mechanics and Rock Mechanics (IBF), Karlsruhe Institute of Technology (KIT), Engler-Bunte-Ring 14, 76131 Karlsruhe, Baden-Württemberg, Germany

1 Introduction

The reliability and reproducibility of soil-mechanical testing results depend crucially on the chosen specimen preparation method and the quality of the specimen preparation process itself. The specimen preparation needs generally to be chosen based on the sand's in situ depositional history. Therefore, various preparation methods for granular soils have been developed over the years. Examples include the dry air pluviation out of a singe nozzle, homogeneous dry sand rain using a multiple sieve apparatus, dry air pluviation using a large sand spreader, water pluviation, pluviation with sub-

Published online: 13 June 2026

sequent compaction, dry deposition in the loosest state with subsequent compaction, and moist tamping. These preparation methods lead to different anisotropic microstructures (fabric) of the specimens. Comparisons of corresponding experimental results are well documented and discussed in numerous scientific publications [5, 6, 9, 10, 14–16, 18, 19, 21, 26, 28]. The quality of the specimen is highly sensitive to even minor variations during preparation. Most specimen preparation techniques, particularly the widely used dry air pluviation methods, are typically performed manually, which further exacerbates this issue.

These inconsistencies caused by human operators can lead to spatial inhomogeneities in density and the micromechanical soil fabric, which may significantly affect subsequent experimental results.

Although standardization efforts have improved interlaboratory comparability to some extent, the fundamental challenge of reproducibility and homogeneity of the specimen preparation process itself and therefore of the testing results overall remains. The scattering of the isotropic (density) and anisotropic (fabric) microstructure [12] of sand specimens may, for example, be one reason for documented deviations of experimental results in round-robin tests conducted by different laboratories despite using the same specimen preparation method.

Considering the dry air pluviation technique in particular, subtle differences in the key parameters fall height, deposition intensity (using a multiple sieve apparatus) or nozzle diameter (using a single nozzle), and uniformity of sand flow can strongly influence the achieved density of the specimen [11, 22]. These effects are difficult and only to a certain extend possible to control and reproduce using manual and human-based methods. Experience has shown that with this method, a mean relative density of $0.2 \lesssim I_D \lesssim 1.0$ can be achieved, whereby these values are dependent on the material and should not be understood as strict limits. As discussed in [27], it can be difficult to achieve small densities using the air pluviation method.

However, the reproducibility as well as the homogeneity of density and fabric of manually prepared air-pluviated specimens is hard to achieve. The later is shown in section 3.

It should also be mentioned that manual specimen preparation is time-consuming and therefore incurs high costs, especially for large and very dense specimens. Note that the manual process can also be remarkably physically demanding.

Recent advancements in robotic technology offer new possibilities such as the here-proposed Robotic Automated Specimen Preparation (RASP). Especially the so-called collaborative robots (Cobot), which can work alongside humans in a shared workspace without the need for physical barriers (such as protective fences), offer a simple and relatively cost-effective opportunity for automating processes [4].

These robots typically exhibit a repeat accuracy in the range of 0.01 - 0.1 mm and are therefore substantially more accurate than manual handling. They provide programmable, traceable, and repeatable procedures that can significantly increase repeatability compared to manual operation. However, despite their potential, robotic systems have only been used a few times in geotechnical research. For example, [2, 7, 20] used an industrial robot as a loading device in the context of physical model testing.

This study introduces and evaluates a Robotic Automated Specimen Preparation (RASP) method for the dry air pluviation technique out of a single nozzle using a conventional six-axis collaborative robot. More than 80 cylindrical sand specimens with a diameter of $D = 10$ cm and a height of $H = 20$ cm were produced. After the preparation, the local density distribution in the specimen is determined in 10 layers across the height of the specimen. Three deposition patterns (concentric, serpentine, and enlarged serpentine) are tested for two different granular materials (Karlsruhe sand (KS) and Karlsruhe fine sand (KFS)) under controlled variations of the nozzle diameter, fall height, and nozzle velocity. The results are compared against specimens prepared manually by human operators with varying levels of experience. The study also examines some special effects, such as a non-constant fall height or the effect of the base plate on the achieved local density.

The RASP method is shown to produce significantly more homogeneous and reproducible specimens compared to those prepared manually. The reproducibility, homogeneity, and practical potential of RASP are demonstrated and establish its readiness for future applications in soil-mechanical laboratories worldwide.

2 The Robotic Automated Specimen Preparation (RASP) method

In this section, the Robotic Automated Specimen Preparation (RASP) method is introduced. A Lexium Cobot arm (LXMRL12S0000) with a 12 kg payload and a 1327 mm working radius is used. The Cobot arm has a positioning accuracy of 0.02 mm and six degrees of freedom. The system is controlled using a Lexium Cobot Cabinet controller (LXMRL12C1000). The EcoStruxure Cobot Expert software, installed on a personal computer, is used to operate the whole system. A funnel with a replaceable nozzle is placed at the tool end under a sand hopper with a diameter of 10 cm and a height of 30 cm. The mass flow is started manually. The cobot is mounted on a solid table, mechanically decoupled from the specimen mold. The whole device is shown in Figure 1. The notation used within this study and the specimen mold is schematically visualized in Figure 2.

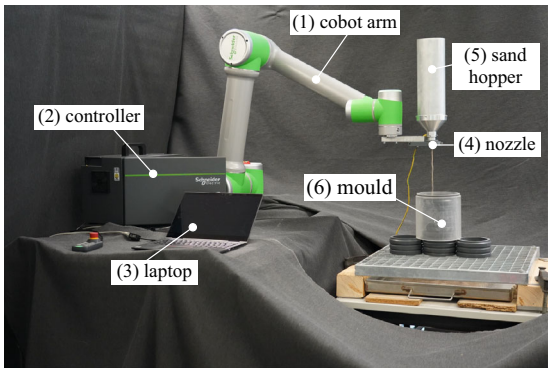

Fig. 1 RASP device for the dry air pluviation out of a single nozzle using a conventional cobot system consisting of: a (1) cobot arm with a (2) controller, a (3) laptop running the operating software, a single replaceable (4) nozzle, a (5) sand hopper, and a specimen (6) mold

Cylindrical soil specimens with a diameter of $D = 10$ cm and a height of $H = 20$ cm are prepared. The specimens are prepared in a mold consisting of a base PVC plate and 10 stackable PVC rings, each with a hight of h_r cm and an inner diameter of $D = 10$ cm. The rings were designed to be self-centering and stackable without the need for screws or any additional mechanical fixtures.

After preparation, the PVC rings can be removed one after the other with minimal disturbance of the soil in the rings below. By leveling the sand along the edge of the current ring on top, the dry mass of the sand inside the ring that has been removed can be determined precisely. The vertical local density distribution inside the specimen can be determined by repeating this procedure for every PVC ring. To simplify the process, the PVC base plate is positioned on a steel grid so that sand grains falling through can be collected in a container and weighed. The described process is shown for one ring in Figure 3.

The dry density ρ_d is then calculated for each ring i:

$$\rho_{\mathrm{d},i} = \frac{m_{\mathrm{d},i}}{V_i} = \frac{4m_{\mathrm{d},i}}{\pi D^2 h_\mathrm{r}} \,. \tag{1}$$

2.1 Materials

Two quartz sands are considered as experimental materials: Karlsruhe sand (KS) and Karlsruhe fine sand (KFS). Both materials have already been extensively studied in the literature (e.g. [23, 24] for KS and [17, 25, 30] for KFS). Table 1 summarizes the soil characteristics and Figure 4 shows the grain size distributions of both materials.

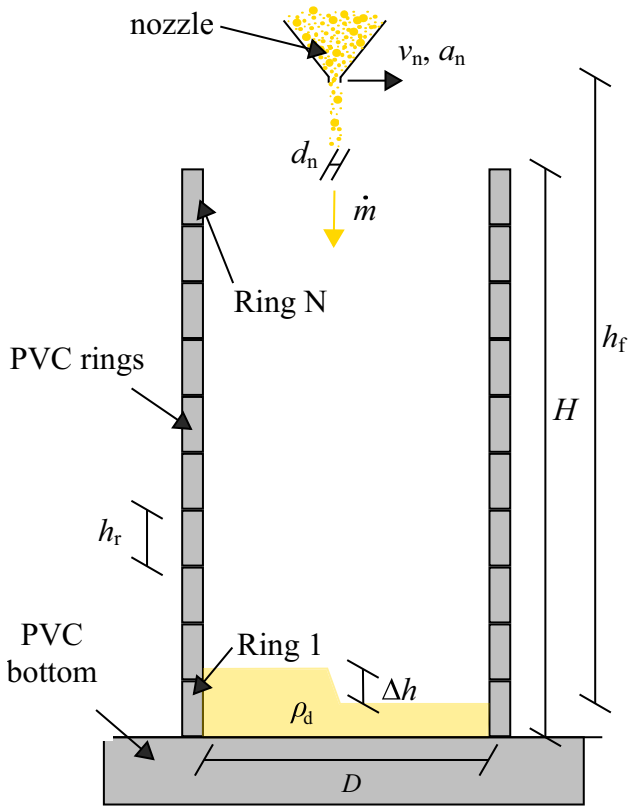

Fig. 2 Schematic drawing of the specimen mold and conventions used in this study

2.2 Flow rate of sand through the nozzle

The mass flow rate $\dot{m} = dm/dt$ of a granular material through the circular nozzle is not affected by the cobot or the human operator (assuming negligible inertia) and is a direct consequence of the interaction between the individual grains, the sand hopper, and the nozzle (diameter and design) itself.

According to Mankoc et al. [13] based on studies with monodisperse spheres, $\dot{m}$ is constant over time if the thickness of the material layer inside the hopper is greater than approximately 1.2 times the diameter of the hopper, and if the diameter of the hopper is greater than 2.5 times the nozzle diameter d_n and also greater than $d_\mathrm{n} + 30d_\mathrm{g}$ with the grain diameter d_g of the monodisperse spheres.

Based on experimental and theoretical investigations, the mass flow rate $\dot{m}$ can be calculated using the law of Beverloo [3]

$$\dot{m} = C\rho_\mathrm{s}\sqrt{g}d_\mathrm{g}^{5/2}\,(R-k)^{5/2} = C'\,(R-k)^{5/2} \tag{2}$$

with the nozzle-to-grain diameter ratio $R = d_\mathrm{n}/d_\mathrm{g}$, the grain density ρ_s, the gravity g and the empirical coefficients k and C resp. C'.

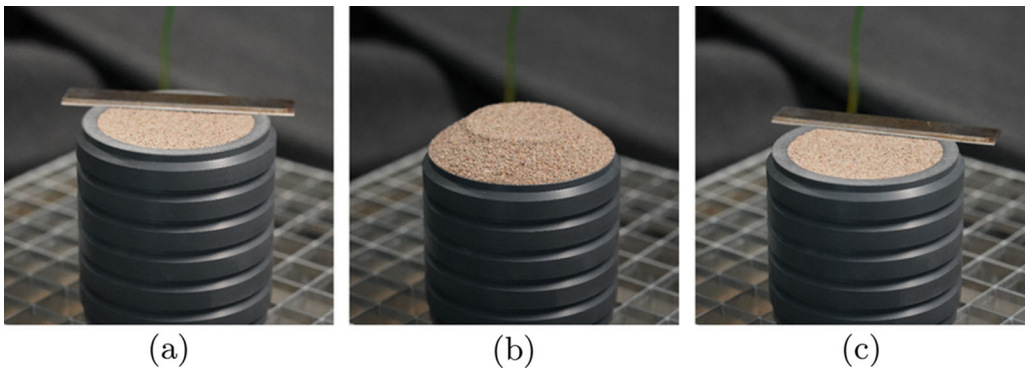

Fig. 3 Process for determining the dry mass and hence the density within a PVC ring: a) leveling the sand before removing the ring, b) removing the ring, and c) leveling the sand after removing the ring

Table 1 Characteristic properties of the Karlsruhe sand (KS) and Karlsruhe fine sand (KFS)

Soil	d_{10}	d_{50}	d_{90}	d_{60}/d_{10}	ρ_s	$\rho_{d,max}$	$\rho_{d,min}$
KS	0.4	0.55	0.9	1.5	2.65	1.71	1.43
KFS	0.09	0.15	0.2	1.5	2.65	1.58	1.29

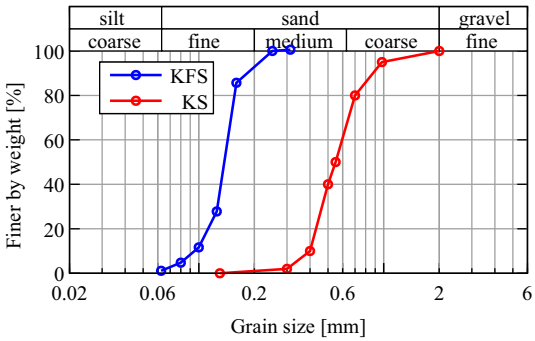

Fig. 4 Grain size distributions of the Karlsruhe sand (KS) and Karlsruhe fine sand (KFS)

As described by [13], Equation 2 is only valid for a small range of R. Therefore, [13] proposed a modified version of Beverloo's law

$$\dot{m} = C^* \left(1 - \frac{1}{2} e^{-b(R-1)}\right) (R-1)^{5/2} \tag{3}$$

with the empirical coefficients C^* and b. Note that the exponent 5/2 is physically justified [13]. [3] considered particles with a grain diameter of $d_g > 0.5$ mm and [13] used particles with $d_g \geq 0.4$ mm assuming that jamming of the nozzle is avoided.

All of these investigations have been conducted using monodisperse spherical particles with a known grain diameter d_g. Natural sand, on the other hand, contains different grain sizes. KFS in particular has significantly smaller grains than those considered in the aforementioned studies. Nevertheless, the results are used and $d_g = d_{50}$ is set for the development of the RASP method.

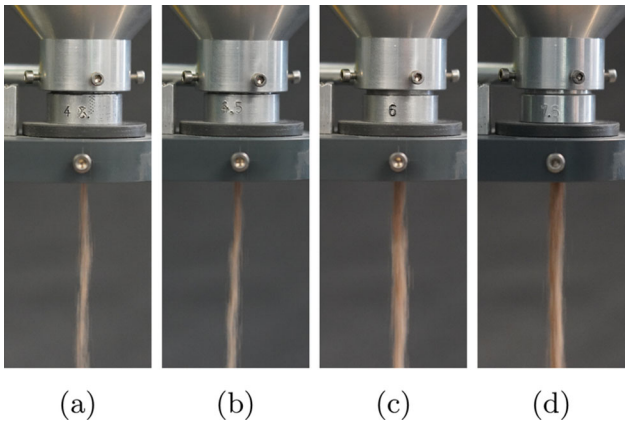

Fig. 5 Mass flow of KS (sand stream) through nozzles with different diameters: a) $d_n = 4.0$ mm, b) $d_n = 4.5$ mm, c) $d_n = 6.0$ mm, and d) $d_n = 7.5$ mm

The measurement of the mass flow rate $\dot{m} = dm/dt = \Delta m/\Delta t$ is performed in this study according to Beverloo et al. [3], conducting three measurements per nozzle diameter and sand type. It simply involves determining the sand mass Δm that has flowed through the nozzle within a certain time period Δt. As the mass flow rate is constant for a specific test setup, the time period Δt has no influence and can be freely chosen. Note that Δt should be long enough to obtain a meaningful measurement of Δm. For both types of sand (KS and KFS) used in this study, mass flow measurements were performed using different nozzles with varying nozzle diameter d_n and therefore varying values of the ratio $R = d_n/d_{50}$. Figure 5 shows the mass flow (sand stream) through four nozzles measured for KS. It is evident that if the nozzle diameter d_n increases, the mass flow becomes larger and the visible sand stream becomes wider and denser.

The measured data were used to calibrate the empirical factors of Equation 2 and Equation 3 using the least squares

Table 2 Calibration of Equation 2 and Equation 3

Soil	C' [g/s]	k [-]	C^* [g/s]	b [-]
KS	$2.52 \cdot 10^{-2}$	1.108	$4.88 \cdot 10^{-2}$	$6.38 \cdot 10^{-4}$
KFS	$7.70 \cdot 10^{-4}$	1.750	$7.34 \cdot 10^{-3}$	0.116

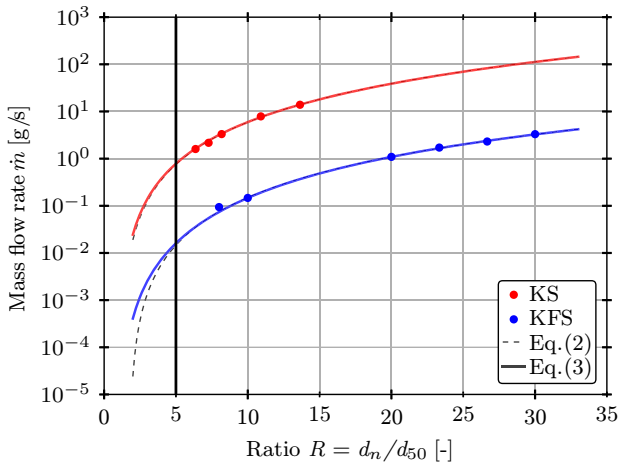

Fig. 6 Mass flow rate $\dot{m}$ for KS and KFS measured three times for each nozzle diameter d_n (overlapping points) and calibration of Equation 2 and Equation 3

method. The calibrated factors are shown in Table 2. It should be noted that even with the same diameter d_n, the construction type of the nozzle itself influences $\dot{m}$ and thus the calibration of the parameters. If a different construction type of the nozzle (e.g. roughness of the material, angle of the funnel and length of the cylindrical outlet) is used, the measurements and the calibration must be repeated accordingly. The experimental results and the calibrated equations are shown in Figure 6. The three measurements per nozzle resulted in almost identical results, as can be seen from the overlapping points in Figure 6. This highly reproducible process is used, for example, in an hourglass and should therefore not be surprising.

In all calibrations, the coefficient of determination is $r^2 > 0.998$ and Equation 2 as well as Equation 3 result in an adequate approximation of the experimental measurements. Noticeable discrepancies between the two mathematical formulations only occur for very small and very large R, which are not investigated in the present study.

According to Zuriguel et al.[29], jamming is to be expected for monodisperse spheres for $R = d_n/d_g = d_n/d_{50} \leq 5$. For natural sand with $d_{max} > d_{50}$, this crucial ratio is expected to be larger. Ensuring that the nozzle is not jammed during the RASP is essential for the process, hence, nozzle diameters with $d_n \gg 5d_{50}$ should be used.

2.3 Procedure

Each Robotic Automated Specimen Preparation (RASP) follows a strict procedure, which is illustrated using a flowchart in Figure 7. First, the nozzle with the diameter d_n, the fall height h_f, the pluviation pattern (described in more detail later), the maximum nozzle velocity v_n and acceleration a_n, as well as the layer rotation angle α and the so-called arc transition l_x must be specified. As described above, the mass flow rate $\dot{m}$ of the granular material through the single nozzle can then be determined.

Once the cobot and pattern parameters have been chosen and $\dot{m}$ is known, the reference point of the nozzle, located in a vertical distance of h_f above the base plate, must be determined. Due to likely production tolerances of the nozzle, the sand stream may not flow exactly vertically from the nozzle. This can lead to a horizontal offset being required between the center of the mold and the center of the pluviation pattern of the nozzle (reference point). Note that both the base plate of the mold and the cobot must be aligned horizontally.

The dry density ρ_d achieved by the specimen preparation depends on all aforementioned parameters, and they must therefore be kept constant during the whole pluviation process to produce homogeneous specimens [1, 22]. To keep the fall height h_f constant as well, the robotic arm must move upwards during the specimen preparation process. This upward movement is practically implemented incrementally with Δh after the completion of every layer of the pluviation pattern and not as a continuous upward movement.

The value of the increment Δh depends on the achieved density of the specimen ρ_d. To avoid a demanding iterative procedure to find Δh, the determination of the so-called target density $\rho_{d,t}$ using the chosen cobot and pattern parameters without an upward movement ($\Delta h = 0$) is proposed. For this purpose, the first and second PVC rings are filled with sand using the desired constant fall height h_f measured from the middle of the second ring to the nozzle. The target density $\rho_{d,t}$ is determined using Equation 1 from the second ring only. As discussed later, the first ring should not be used to measure $\rho_{d,t}$, as the dry mass inside this ring can be strongly influenced by the bottom of the mold (base plate effect).

The increment Δh is given by

$$\Delta h = \frac{4\dot{m}}{\rho_{d,t}\pi D^2}\,\Delta t \tag{4}$$

with the time per layer Δt, assuming that during Δt every grain falls into the mold. It should be noted that Δt can generally be equal to or less than the time required by the cobot for each layer. If the nozzle moves over the edges of the mold, and thus not all grains fall into the latter, Δt is smaller than the time required by the cobot for every layer. In this case, only the time intervals within a layer during which the nozzle

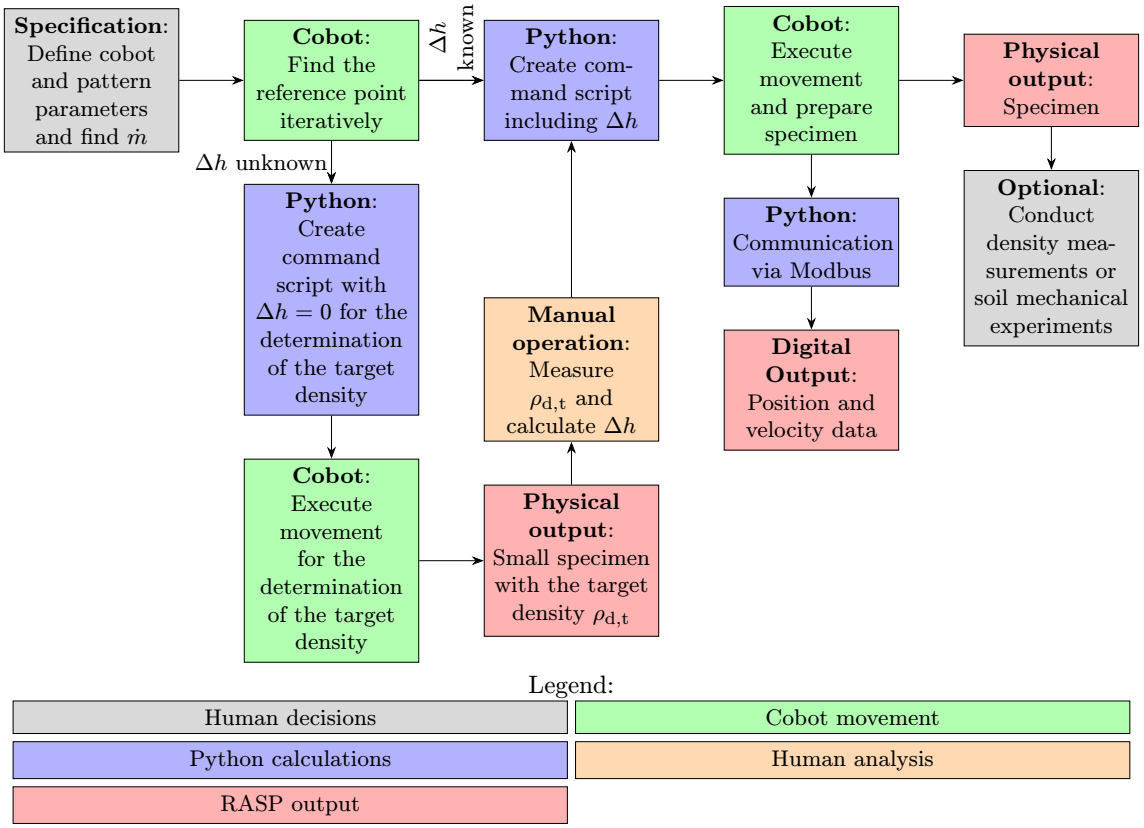

Fig. 7 Flowchart showing the required steps for the RASP using the dry air pluviation technique through a single nozzle

is positioned within the mold are counted. For a cylindrical specimen with a diameter D, $\sqrt{x^2 + y^2} \leq D/2$ must apply for the counted time intervals, see also Figure 14.

By simply measuring h_f at the beginning and end of the RASP, it can be checked whether Δh is correctly determined. The latter is the case if h_f is the same at the beginning and end of the RASP. To generate a homogeneous specimen, all parameters should be chosen such that $\Delta h \ll H$, and, in the case of local density measurement, $\Delta h \ll h_r$ applies. This ensures that the specimen is prepared with a large number of layers.

In the next step, the three-dimensional commands for the movement of the cobot based on the reference point are created. The selected pluviation pattern is executed in several layers. After each layer, the nozzle moves upwards by Δh. Furthermore, the layer patterns above each other are rotated by an angle of $\alpha = 17°$ in a clockwise direction. This value was chosen because a rotation of $\alpha = 17°$ results in a long repetition period of the layer orientation, while still providing a pronounced relative rotation between directly adjacent layers. As a result, identical deposition paths occur only after 360 layers, and systematic superposition of successive layers is effectively avoided. In addition, the transition path between two layers is relatively short and can be neglected for Δt.

The commands for the cobot are created using a Python script. This Python script generates a text file (cobot command script) that can be imported into the control system (EcoStruxure Cobot Expert software) of the cobot. The main components of this command script are the coordinates of the individual points of the desired trajectory of the chosen pluviation pattern and the motion commands between these points. The movement itself consists of a sequence of linear motion commands. For the transition between individual linear motions, so-called arc transitions l_x are incorporated, which round off the trajectory and thus prevent/reduce braking of the cobot arm at the end and accelerating again at the beginning of each linear motion. The impact of the arc transition is evident from a comparison of Figure 10 with Figure 12 to Figure 14. The movement between the specified points is performed by the cobot itself, following a uniformly accelerated motion as a function of the specified maximum nozzle velocity v_n, nozzle acceleration a_n, and arc transition l_x.

Once the cobot command script is created, the actual specimen production can begin. During the specimen preparation, the cobot can export position and velocity data via a Modbus communication protocol, which can be used as digital output during the procedure. This data is saved in a text file using another Python script and enables the trajectory of the

preparation process to be reconstructed at a later time. This provides a basis for quality assurance and documentation.

The procedure described for the RASP method can, in principle, be easily transferred to other robotic systems. Theoretically, even a simple 3-axis system could be used. In this context, it is important that the respective robotic system enables continuous movement along any three-dimensional trajectory. Therefore, only the command script needs to be adapted to the respective robot control system. Logging robot data during RASP via the digital output is not mandatory and can be omitted for the sake of simplicity. It should be noted that collaborative robotic systems can pose significant risks to human users/operators if the system is operated incorrectly [4]. The authors consider appropriate safety training to be essential.

3 Experimental results

Overall, over 80 specimens under variation of the

- pluviation pattern (concentric (C), serpentine (S), and enlarged serpentine (ES))
- material (KS and KFS)
- nozzle diameter d_n (3.0, 4.0, 4.5, 6.0, and 7.5 mm)
- fall height h_f (15, 25, and 35 cm)
- nozzle velocity v_n (6, 8, and 10 cm/s)
- base plate made of PVC without a specification, with one membrane (1 M), with two membranes (2 M), with one membrane and lubrication (1LM), and with a porous stone (PS)

keeping the

- nozzle acceleration $a_n = 40$ cm/s^2
- layer rotation angle $\alpha = 17°$
- arc transition $l_\mathrm{x} = 1$ mm

constant, have been automatically prepared during the development of the presented RASP method. It should be noted that only the key insights are shown hereafter, each of which has been confirmed by further variations and tests which are not shown in detail but are considered statistically in subsection 3.6. The tests using the RASP method are labeled using the system:

$$< \text{pattern} > - < \text{material} > - < d_\mathrm{n} > - < h_\mathrm{f} > - < v_\mathrm{n} > - < \text{notes} > \ .$$

For example, the test C-KFS−6.0-25-8 represents a RASP test with the concentric pattern using Karlsruhe fine sand, a nozzle diameter of $d_\mathrm{n} = 6.0$ mm, a fall height of $h_\mathrm{f} = 25$ cm, and a maximum nozzle velocity of $v_\mathrm{n} = 8$ cm/s.

Additionally, 12 specimens have been produced by humans (H) with different levels of experience (expert (E), intermediate (I), newbie (N)). The newbie is a trainee with no experience in soil mechanics laboratories. The intermediate is the second author and the expert is a lab technician with over 15 years of professional experience in the soil mechanical lab of the Institute for Soil and Rock Mechanics (IBF) of the Karlsruhe Institute for Technology (KIT), who prepared, for example, specimens for experiments shown in [8, 17, 25]. All human operators were only told the desired constant fall height $h_\mathrm{f} = 25$ cm. Nozzle diameter was preset. The labeling of the manually prepared specimens corresponds to

$$\mathrm{H}- < \text{experience} > - < \text{material} > - < d_\mathrm{n} > \ .$$

For example, the test H-E-KS−4.5 is conducted by the expert using Karlsruhe sand, and a nozzle diameter of $d_\mathrm{n} = 4.5$ mm. It should be noted that, during the manual specimen preparation process, the nozzle does not follow a predetermined pluviation pattern. Rather, the actual movement of the nozzle during the manual process depends on the operator and also changes during the specimen preparation. Different operators naturally use different non-quantifiable techniques. It should also be noted that the operator may attempt to compensate for any inhomogeneities by adjusting their movements (including tilting the funnel). Each test (RASP and human) was performed twice.

The specimen preparation results are presented using the relative density for each PVC ring i:

$$I_{\mathrm{D},i} = \frac{\rho_{\mathrm{d},i} - \rho_{\mathrm{d,min}}}{\rho_{\mathrm{d,max}} - \rho_{\mathrm{d,min}}} \ . \tag{5}$$

First, Figure 8 presents the vertical distribution of the relative density for human-made KS-specimens for two different nozzle diameters and varying levels of experience of the human operator. Corresponding results for specimens produced automatically with the same fall height of $h_\mathrm{f} = 25$ cm and varying nozzle diameters are shown in Figure 9.

The results reveal that RASP significantly improves the homogeneity of the densities achieved along the specimen height within each specimen as well as the reproducibility of the results. This general observation is valid irrespective of the experience of the lab technician.

To validate these observations, the mean value

$$\bar{I}_\mathrm{D} = \frac{1}{N-2} \sum_{i=2}^{N-1} I_{\mathrm{D},i} \tag{6}$$

and the coefficient of variation

$$CV = \frac{s}{\bar{I}_\mathrm{D}} \tag{7}$$

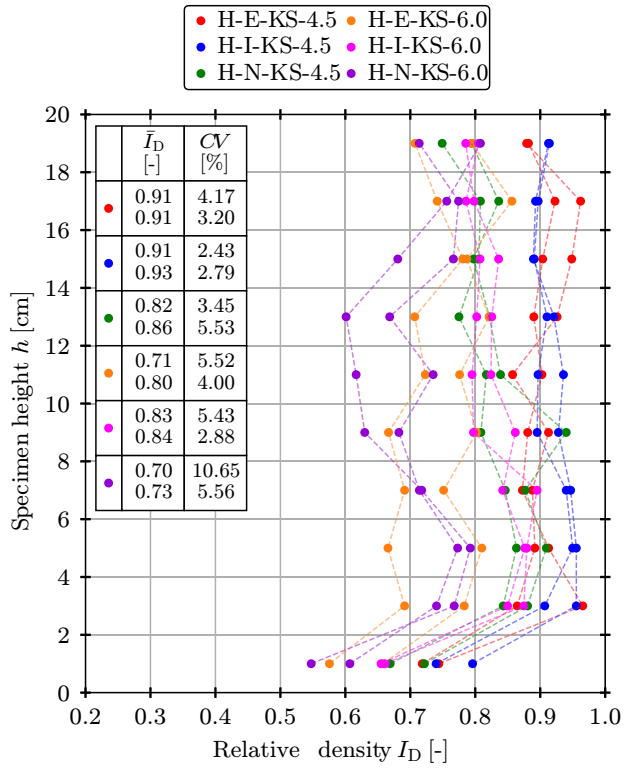

Fig. 8 Relative density distribution in human-made KS-specimens with varying levels of experience of the lab technician using different nozzle diameters

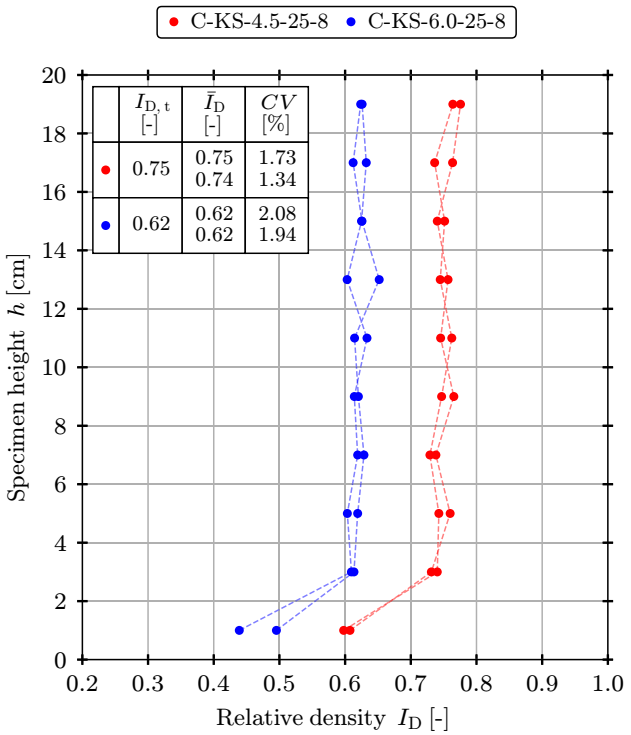

Fig. 9 Relative density distribution in RASP-made KS-specimens with varying nozzle diameters

using the standard deviation

$$s = \sqrt{\frac{1}{N-3}\sum_{i=2}^{N-1}\left(I_{D,i} - \bar{I}_D\right)^2} \tag{8}$$

of the achieved relative densities of ring $i = 2$ to ring $i = N - 1$ are determined for each specimen preparation and stated in the corresponding figures. For the RASP specimens, the relative target density $I_{D,t}$, calculated using the target density $\rho_{d,t}$, is also mentioned. Note that the bottom and top PVC rings (ring 1 and ring N) are omitted in the statistics to exclude boundary effects.

With regard to the following results, it should be noted that the method used to measure the density distribution is also subjected to errors. Although this manual process was carried out with the greatest care, minor errors in mass determination and disturbance of the specimen can not be excluded.

Both the coefficient of variation CV within every individual specimen and the deviation of the mean density $\bar{I}_D$ of the two repeated specimen preparations are significantly larger for the human-made specimens than for the RASP specimens, see also Table 3. In the discussed specimens in Figure 8 and Figure 9, the maximum achieved coefficient of variation is measured in one of the tests H-N-KS−6.0, done by the newbie with $CV = 10.65\%$. Even the expert could only achieve a coefficient of variation of $CV = 3.20\%$ in the best case scenario in one of the tests H-E-KS−4.5. Interestingly, the intermediate achieves an even better value of $CV = 2.43\%$ in an H-I-KS−4.5 specimen. The minimum achieved coefficient of variation is reached using the RASP in one test C-KS−4.5-25-8 with $CV = 1.34\%$. The largest difference in the mean density $\bar{I}_D$ between the two repeated tests $\Delta\bar{I}_D = |\bar{I}_{D,1} - \bar{I}_{D,2}|$ is surprisingly achieved by the expert with $\Delta\bar{I}_D = 0.09$ for the tests H-E-KS−6.0. The reproducibility is significantly improved using the proposed RASP method, where $\Delta\bar{I}_D \leq 0.01$ is observed for all repetitive tests. Additionally, in the RASP tests, the target density corresponds to the achieved density ($I_{D,t} \approx \bar{I}_D$), confirming the proposed RASP procedure.

Interestingly, in all tests, the expert achieved denser specimens than the beginner and also than the robot, which emphasizes the influence of the human operator on the specimen preparation result.

As expected from the literature [1, 22], a larger nozzle diameter results in a lower density, irrespective of whether the specimen is manually or automatically prepared.

Another observation and similarity between manually and automatically prepared specimens is the significantly lower density in the PVC ring located at the bottom of the mold. The comparatively hard impact of the grains falling on the bottom of the mold leads to looser density than if the grains fall on sand. This base plate effect is discussed in detail later.

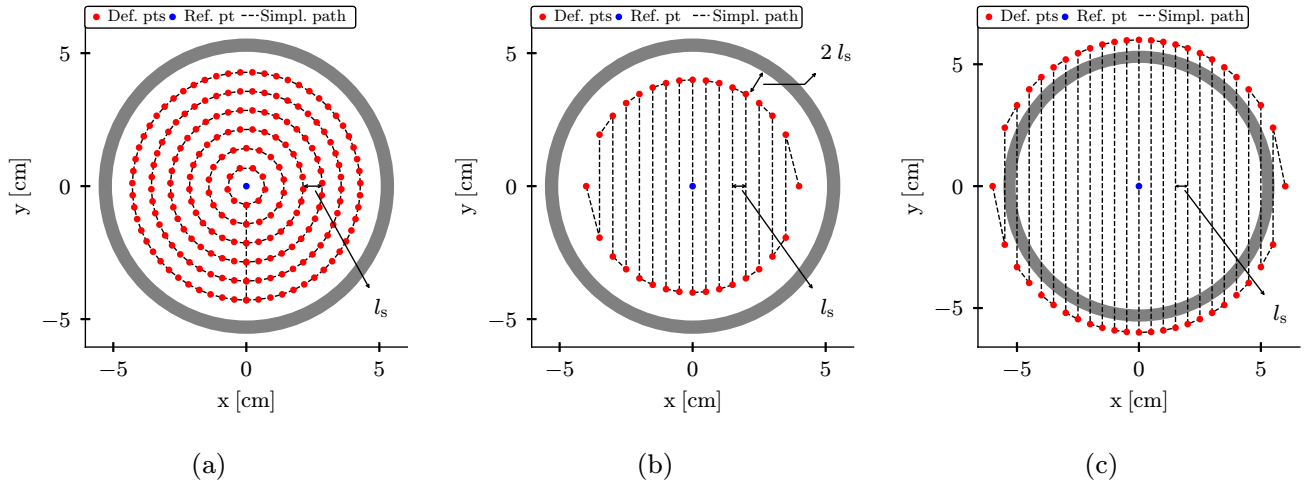

Fig. 10 Defined points and simplest path for $l_x = 0$ in the first layer of the: a) concentric (C) pattern, b) serpentine (S) pattern, and c) enlarged serpentine (ES) pattern

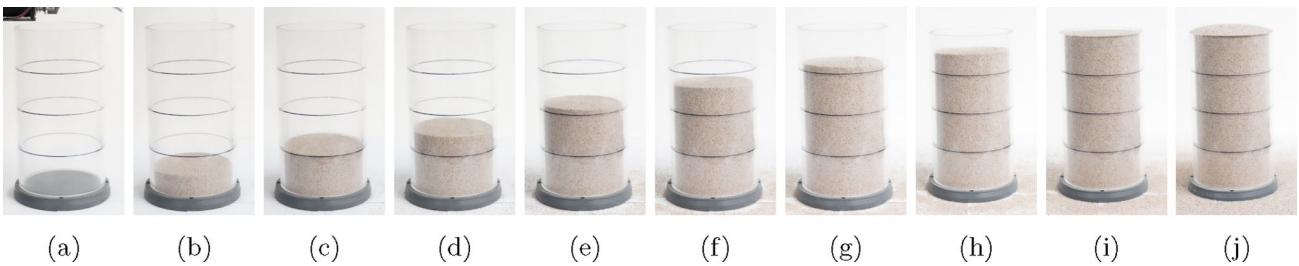

Fig. 11 Sand surface and evolution of the specimen during the RASP process for a specimen prepared with the serpentine pattern

3.1 Influence of the pluviation pattern

Three different pluviation patterns, a concentric (C), a serpentine (S), and an enlarged serpentine (ES) pattern, are investigated for the RASP-made specimens.

The predefined points in the command script and the simplest pluviation pattern for $l_x = 0$ (straight lines connecting the predefined points) are shown for the concentric (C) pattern in Figure 10a, for the serpentine (S) pattern in Figure 10b, and for the enlarged serpentine (ES) pattern in Figure 10c. These figures also indicate the path spacing l_s, which can be interpreted as a characteristic scale for the respective pattern. l_s varies for the different patterns. $l_s \leq 30d_{50}$ is used to ensure a nearly flat surface of every pluviated sand layer. However, it should be noted that this flat surface is not necessarily ensured when the stated recommendation for l_s is adopted. The flatness of the sand surface during the RASP process must be visually checked for each material and parameter combination. To demonstrate the layerwise flatness of the sand surface during the RASP process, a specimen was prepared using the serpentine pattern in a transparent mold instead of the PVC rings described above. The RASP parameters were chosen in accordance with the preparation parameters of specimen S-KS−4.5-25-8. Figure 11 shows images of the sand surface and the evolution of the specimen during the RASP process. As intended, the surface is always sufficiently flat.

The cobot performs linear movement commands between the predefined points shown in Figure 10. This approach is ideal for the serpentine pattern, as rather few points are required per layer. However, a large number of points is required to perform the concentric pattern with linear movement commands. Note that too many points and too many decimal digits of the coordinates may lead to issues with the control system. Alternatively, circular movements could also be used for the concentric pattern to reduce the required number of points. A potential disadvantage of the concentric pattern lies in the circular path itself, which requires an acceleration (perpendicular to the direction of movement) even at a constant norm of the nozzle velocity v_n. Due to the inertia of the grains, the nozzle pattern may only be partially transferred to the specimen surface, especially at high nozzle velocities.

To discuss the pluviation patterns in detail, the position and velocity data exported from the cobot during the specimen preparation via a Modbus communication are visualized for the first three layers for the tests C-KS−4.5-25-8 (concentric pattern) in Figure 12, for the tests S-KS−4.5-25-8

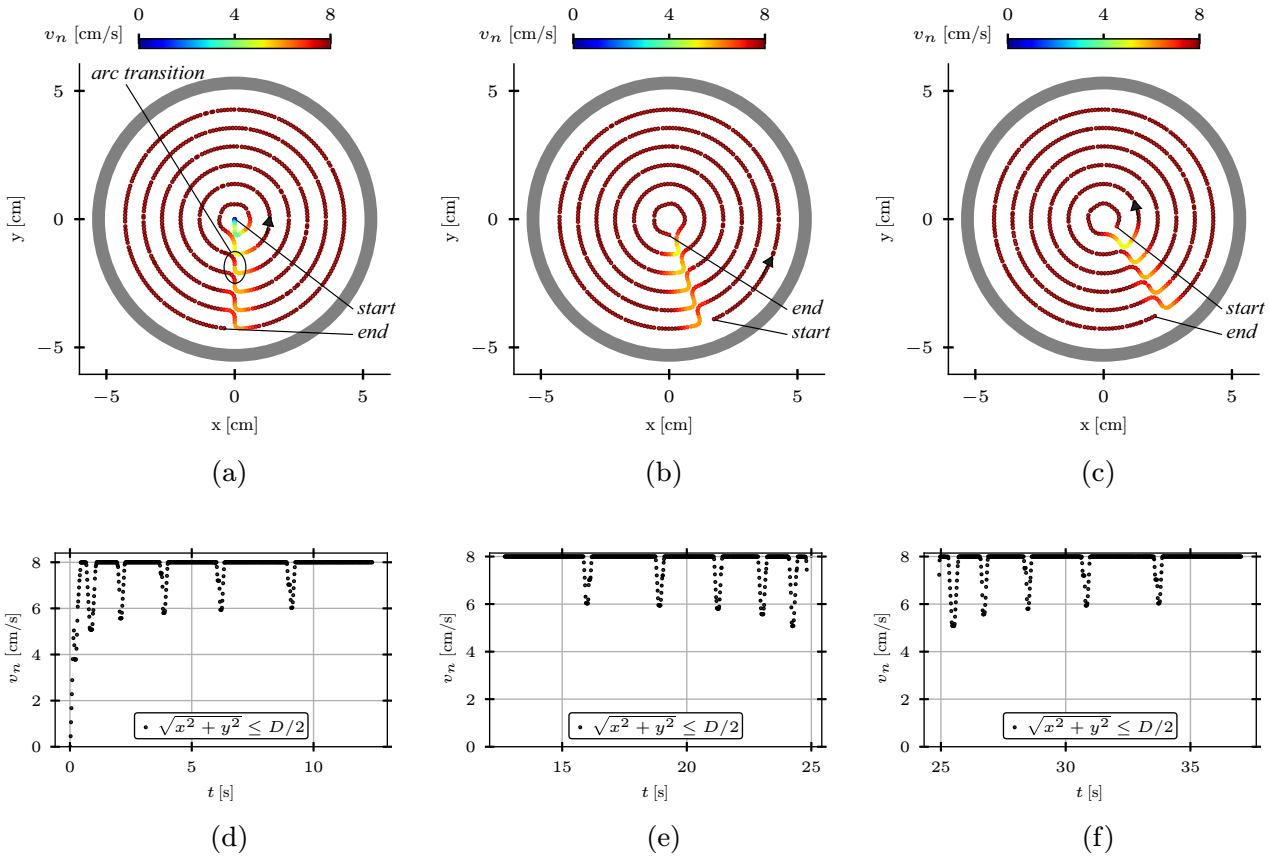

Fig. 12 First three layers of the tests C-KS−4.5-25-8 with the concentric (C) pluviation pattern: norm of the nozzle velocity v_n as a function of the a) to c) nozzle position and d) to f) specimen preparation time t

(serpentine pattern) in Figure 13, and for the tests ES-KS−4.5-25-8 (enlarged serpentine pattern) in Figure 14.

The top row of these figures (a to c) shows the norm of the nozzle velocity v_n as a function of the nozzle position in x-y coordinates. It should be noted that this data represents the movement of the nozzle. Due to inertia and the fall height, the grains reach the specimen surface with a slightly different pattern. Currently, the latter cannot be documented.

It can be seen that the cobot executes the desired pluviation pattern through the defined points shown in Figure 10, layer by layer. However, due to the specified arc transition $l_x = 1$ mm, the cobot does not reach exactly the defined points, but rounds off the path slightly. Therefore, the norm of the nozzle velocity corresponds to the maximum norm of the nozzle velocity during almost the entire pluviation of each layer. Without the arc transition, the nozzle would follow the simplified paths exactly shown in Figure 10 and there would be a temporary zero velocity at the defined points due to acceleration and deceleration of the cobot. This is confirmed by the bottom rows of Figure 12, Figure 13, and Figure 14 (d to f), which show the norm of the nozzle velocity v_n as a function of the specimen preparation time t. In these figures, black dots correspond to a position of the nozzle inside the mold ($\sqrt{x^2+y^2} < D/2$) and gray dots correspond to a position of the nozzle outside the mold. The latter only occurs using the enlarged serpentine (ES) pattern in Figure 14, where the predefined points lie outside the mold.

The cobot only needs to reduce its velocity temporarily whenever it changes its path sharply. The time required by the cobot to decelerate or accelerate depends on the given norm of the nozzle acceleration a_n. In all tests shown in this paper, $a_n = 40$ cm/s^2 is chosen. Previous tests have shown that a_n has a negligible influence on the results (not shown). Nevertheless, this relatively large norm of the nozzle acceleration a_n, combined with the norm of the nozzle velocity v_n and the selected arc transition l_x, results in a relatively pronounced impact on the nozzle when the movement direction changes. This impact is still tolerable for the entire system. For small diameters, where blockages are expected, this impact can resolve temporary blockages.

For the concentric (C) pattern, the reduction of the nozzle velocity occurs at the transition between individual circles. In the serpentine (S) pattern, the velocity reduction can be seen at the end of a linear motion when the direction changes.

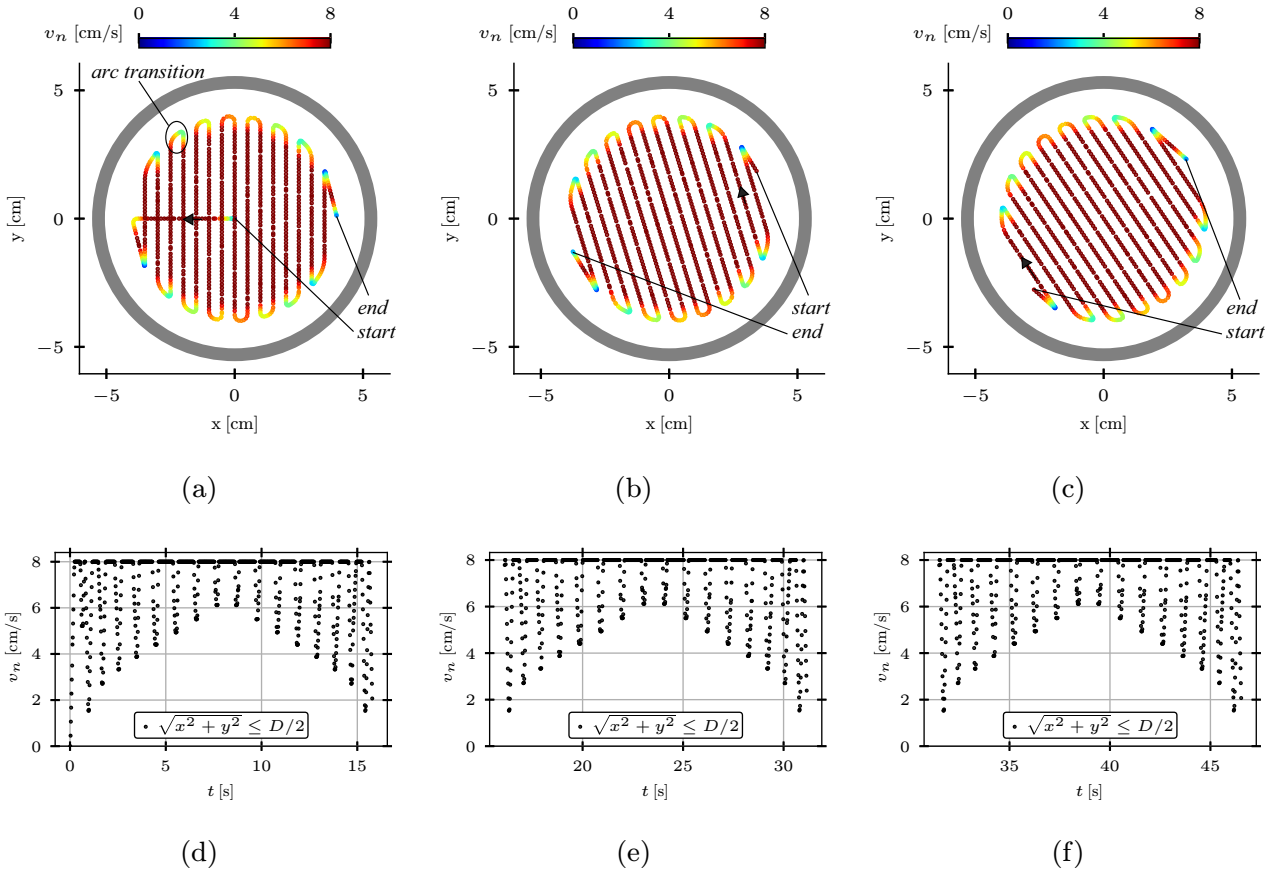

Fig. 13 First three layers of the tests S-KS−4.5-25-8 with the serpentine (S) pluviation pattern: norm of the nozzle velocity v_n as a function of the a) to c) nozzle position and d) to f) specimen preparation time t

Here, the theoretical advantage of the enlarged serpentine (ES) pattern becomes apparent. The cobot also reduces its velocity and accelerates upon a change in direction, but this occurs when the nozzle is located outside the mold and the grains that fall out of the nozzle during the accelerating periods do not fall into the mold. In order to obtain a sharp separation between the falling grains inside and outside the mold, the upper PVC ring is provided with a sharp edge. Note that for these tests, the determination of Δt is nontrivial and is not simply calculated using $\Delta t = t_{\text{End, Layer i}} - t_{\text{Start, Layer i}}$ as it can be done is for the aforementioned concentric and serpentine pluviation patterns. For the ES pattern, Δt is the total time in one layer during which the nozzle is positioned above the mold ($\sqrt{x^2+y^2} \leq D/2$). All corresponding time points satisfying $\sqrt{x^2+y^2} \leq D/2$ are highlighted in dark color in Figure 14 (bottom row).

For the tests C-KS−4.5-25-8, the time per layer is approximately $\Delta t = 12.14$ s, which, using $\dot{m}$ and $\rho_{\text{d,t}}$, results in a value of $\Delta h = 3.18$ mm. For the tests S-KS−4.5-25-8 applies $\Delta t = 15.02$ s and $\Delta h = 3.89$ mm and for the tests ES-KS-4.5-25-8 applies $\Delta t = 17.90$ s, and $\Delta h = 4.69$ mm.

In addition, Figure 12 to Figure 14 demonstrate the rotation of the pluviation patterns by $\alpha = 17°$ for each layer. It should be noted that the upward movement, which is also rounded due to the arc transition l_x, is not visible in the figures. It can only be inferred from the offset of the end point of one layer with respect to the start point of the next layer.

The actual three-dimensional trajectories for the tests C-KS−4.5-25-8 and S-KS−4.5-25-8 are shown in Figure 15 and Figure 16. The layers at a height of $h = 0$, $h \approx H/4 = 5$ cm, $h \approx H/2 = 10$ cm, $h \approx 3H/4 = 15$ cm, and $h \approx H = 20$ cm are highlighted in colors. The rest of the path is shaded in gray. This three-dimensional representation illustrates the crowdedness of the overall movement of the robotic arm. It can be seen that the movements of the concentric patterns in each plane overlap each other, whereas in the serpentine pattern, the linear movements of each layer intersect with the adjacent layers. To ensure that the mold is thoroughly filled and that even the top layer of the specimen is equally compacted, the specimen is sufficiently buried with sand. Doing so, a comparable compaction of the soil in the top layer compared to the one in deeper layers is guaranteed.

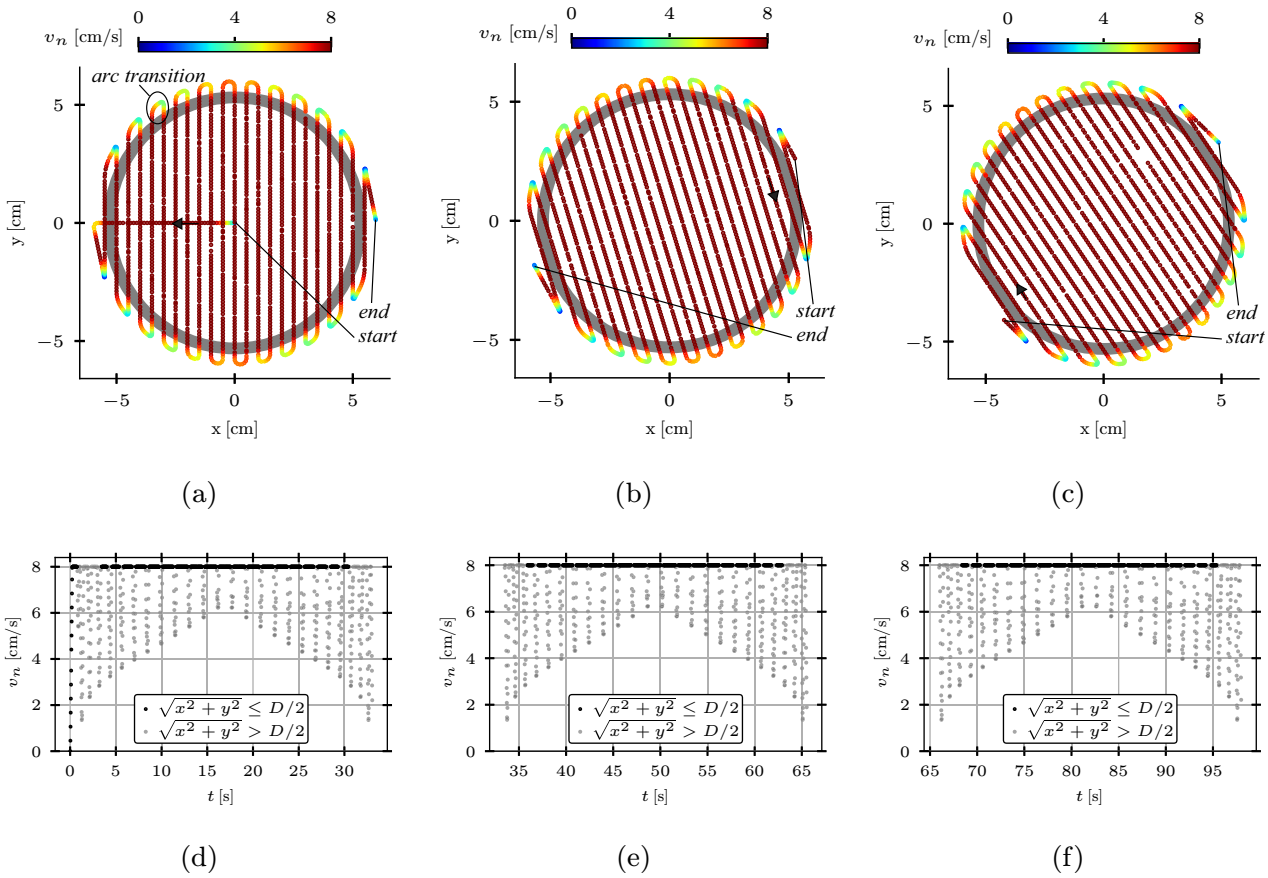

Fig. 14 First three layers of the tests ES-KS−4.5-25-8 with the enlarged serpentine (ES) pluviation pattern: norm of the nozzle velocity v_n as a function of the a) to c) nozzle position and d) to f) specimen preparation time t

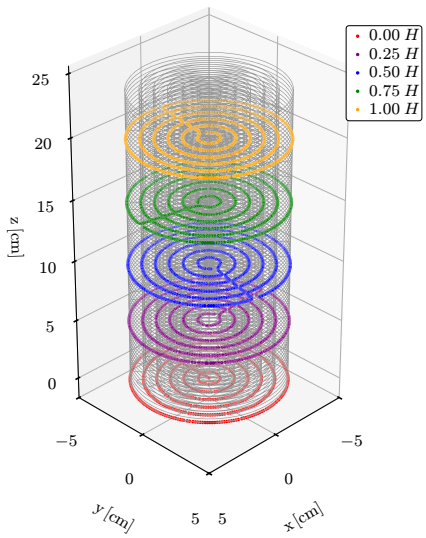

Fig. 15 3D nozzle trajectory of the tests C-KS−4.5-25-8 (concentric pattern)

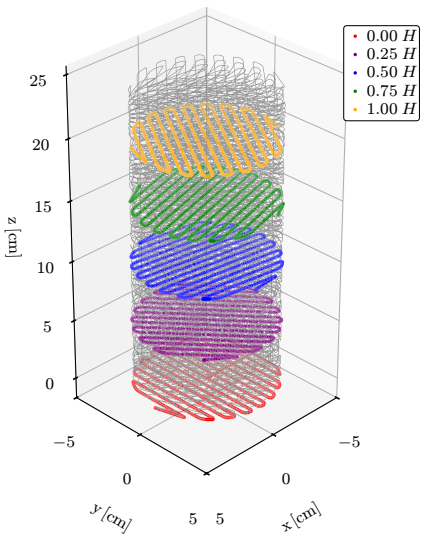

Fig. 16 3D nozzle trajectory of the tests S-KS−4.5-25-8 (serpentine pattern)

Therefore, total vertical displacement $\sum \Delta h > H$ of the nozzle must be greater than the height of the mold.

Figure 17 shows the density distributions of the resulting specimens under variation of the pluviation pattern. First, it

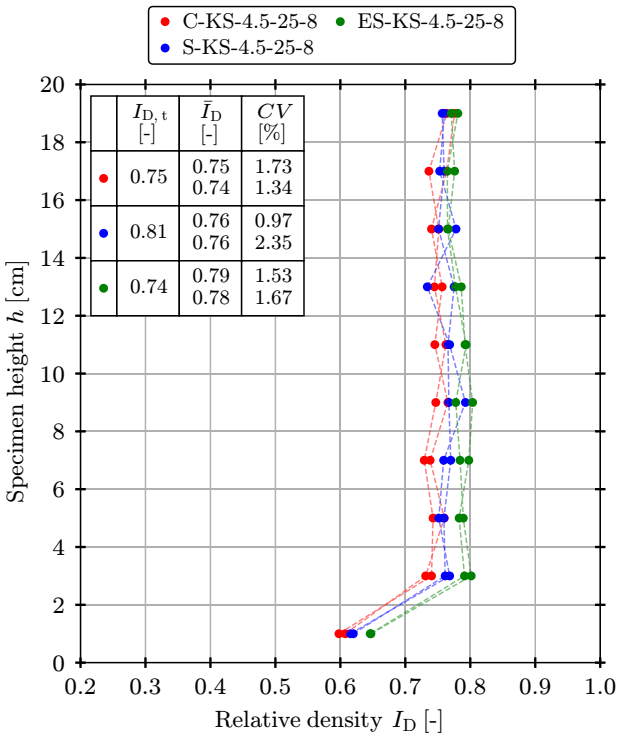

Fig. 17 Relative density distribution in RASP-made KS-specimens for three pluviation patterns

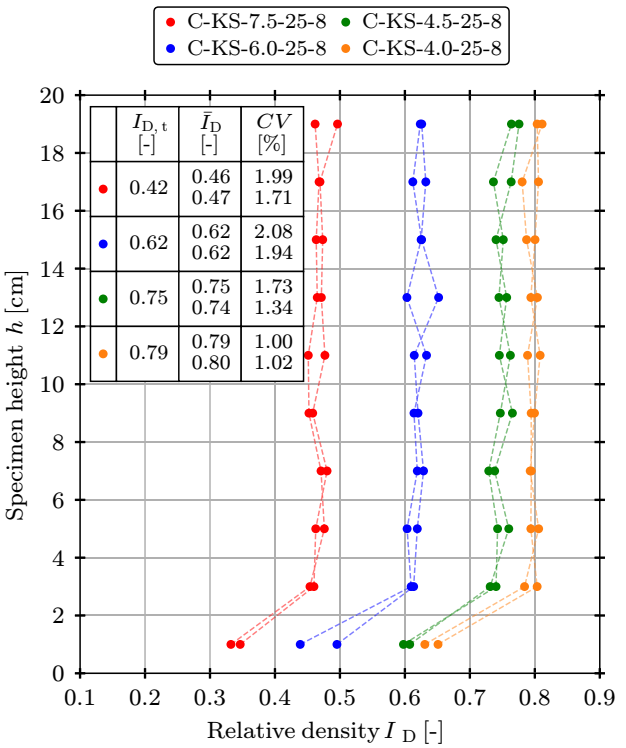

Fig. 18 Relative density distribution in RASP-made KS-specimens with varying nozzle diameters

should be noted that all three patterns produce significantly more homogeneous and reproducible specimens than manual preparation. The homogeneity (CV) and reproducibility ($\Delta\bar{I}_D$) are of the same order of magnitude for all pluviation patterns. Interestingly, the ES pattern leads to the highest density ($\bar{I}_D = 0.79$) and the C pattern to the lowest density ($\bar{I}_D = 0.74$). It is also worth noting that the differences between the target density and the achieved density are significantly greater for the S and ES patterns ($\approx 5\%$) than for the C pattern ($< 1\%$). One additional shortcoming of the ES pattern should be mentioned: compared to the other patterns, the specimen preparation needs significantly more time, and more material must be filled into the sand hopper.

Overall, the reproducibility of specimens prepared using the RASP method is independent of the pluviation pattern, although the latter slightly influences the achieved density. The concentric pattern is used in the following.

3.2 Influence of the nozzle diameter and fall height

The nozzle diameter d_n affects the achievable density of the specimen decisively. This is shown in detail in Figure 18, where the diameter d_n is systematically varied ($d_n = 4.0$ mm to $d_n = 7.5$ mm). The smaller the nozzle diameter, the greater the achieved density. For the nozzles mentioned, with a fall height of 25 cm, relative densities between $\bar{I}_D = 0.46$ and $\bar{I}_D = 0.80$ are achieved. However, the usable nozzle diameter is limited, as small diameters can cause the nozzle to become blocked. Figure 18 also demonstrates that the coefficient of variation (CV) is higher at lower densities. Although the absolute deviation (measured using the standard deviation (s)) is nearly independent of the density (not shown), smaller mean values $\bar{I}_D$ result in larger relative deviations expressed using the coefficient of variation. Overall, $CV < 2.08\%$ applies for the specimens in Figure 18 and they can therefore be considered to be highly homogeneous.

The fall height h_f also has a decisive influence on the achieved density. Figure 19 presents experimental results with varying fall height ($h_f = 25$ cm and $h_f = 35$ cm). An increased fall height leads to an increased density of the specimen.

Additionally to the test with desired nearly constant fall height h_f ($\Delta h \neq 0$) during the specimen preparation process, some tests have also been conducted keeping the nozzle at a constant (c) global height above the base plate during the overall specimen preparation ($\Delta h = 0$). In this case, the given value of h_f only applies immediately at the beginning of the pluviation. Consequently, the fall height h_f decreases during the pluviation process. The more soil mass has already been pluviated into the mold, the lower h_f during the process. As can be seen in Figure 19, this results in a decrease in density with increasing specimen height. The effect is more pronounced if the initial fall height is smaller. For example,

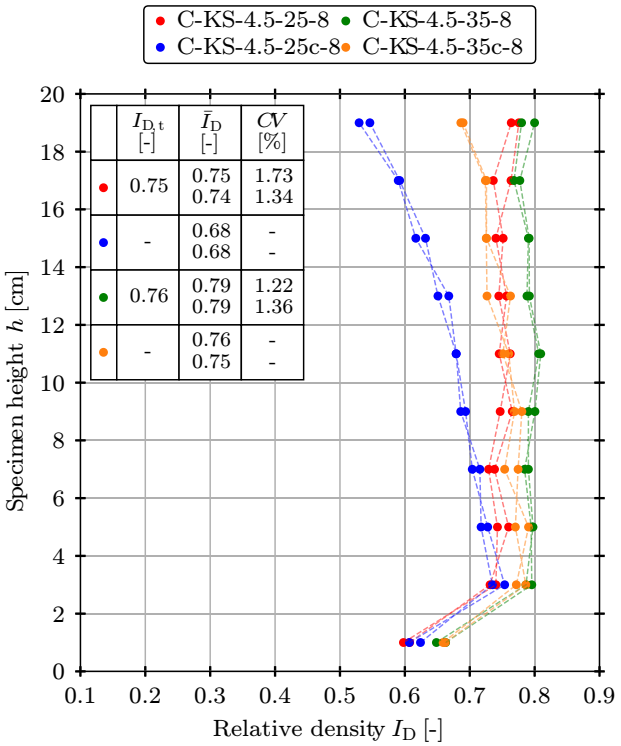

Fig. 19 Relative density distribution in RASP-made KS-specimens with varying fall height h_f

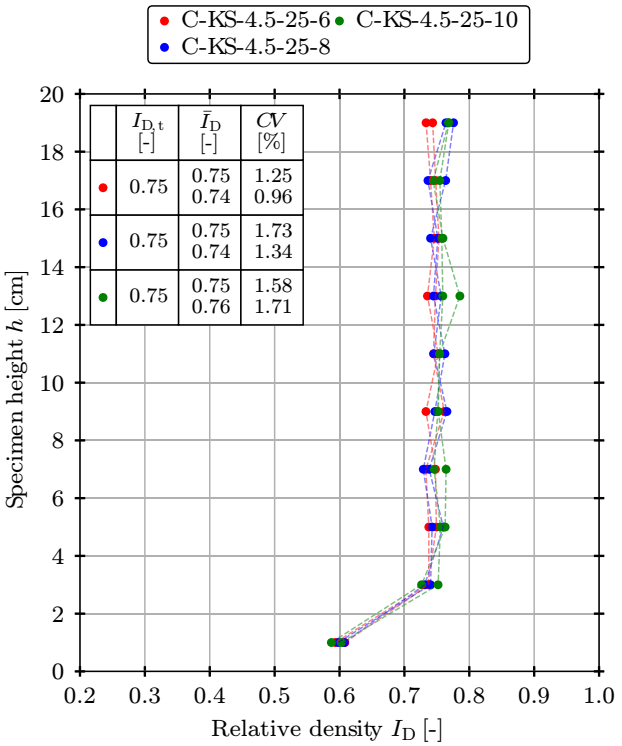

Fig. 20 Relative density distribution in RASP-made KS-specimens with varying norm of the nozzle velocity v_n

the specimens C-KS−4.5-25c-8 have a relative density of $I_D \approx 0.75$ at the bottom and $I_D \approx 0.55$ at the top. The average relative density $\bar{I}_D \approx 0.68$ obviously has only limited relevance in these specimens.

The observations regarding the influence of the fall height and nozzle diameter on the achieved density are consistent with the literature [1, 22]. Vaid and Negussey [22] explain that increasing the fall height leads to a denser specimen only up to a certain h_f, beyond which the grains reach their so-called terminal velocity. Once this fall height is reached, further increases in h_f no longer affect the resulting density.

3.3 Influence of the nozzle velocity

As shown in Figure 20, the investigated maximum norm of the nozzle velocity v_n has a minor effect on the achieved density. Values of $v_n = 6$, $v_n = 8$, and $v_n = 10$ cm/s are investigated. A slight trend towards a looser specimen with decreasing v_n can be observed. On the other hand, lower values of v_n lead to a larger Δh (larger Δt at the same $\dot{m}$), which is not desirable. A mean value of $v_n = 8$ cm/s appears to be a good compromise, thus, this norm of the nozzle velocity is chosen for all further tests in this paper.

3.4 Influence of the granular material

So far, only tests with Karlsruhe sand (KS) have been shown. Figure 21 now considers the density distribution for RASP specimens using the significantly finer Karlsruhe fine sand (KFS). Two different fall heights ($h_f = 25$ cm and $h_f = 35$ cm) and two different nozzle diameters ($d_n = 3.0$ mm and $h_n = 4.5$ mm) are considered for the KFS-specimens. It should be noted that due to the finer material, a decreased l_s has been chosen compared to the KS-specimens with the same concentric pluviation pattern. All effects already discussed for KS are confirmed for KFS: an increased fall height and a decreased nozzle diameter lead to an increased density of the specimens. The statistical values CV and ΔI_D fall within the same range already discussed for the RASP of KS-specimens. There is only a minor increased coefficient of variation CV, which can be attributed to a very small trend of a decreased density with increased specimen height shown in Figure 21. It can be assumed that this observation could be improved even further by fine-tuning the RASP parameters. The proposed RASP method is therefore confirmed for various granular materials. It is noteworthy that the previously apparent lower density in the bottom ring in the KS-specimens is not pronounced in the KFS-specimens.

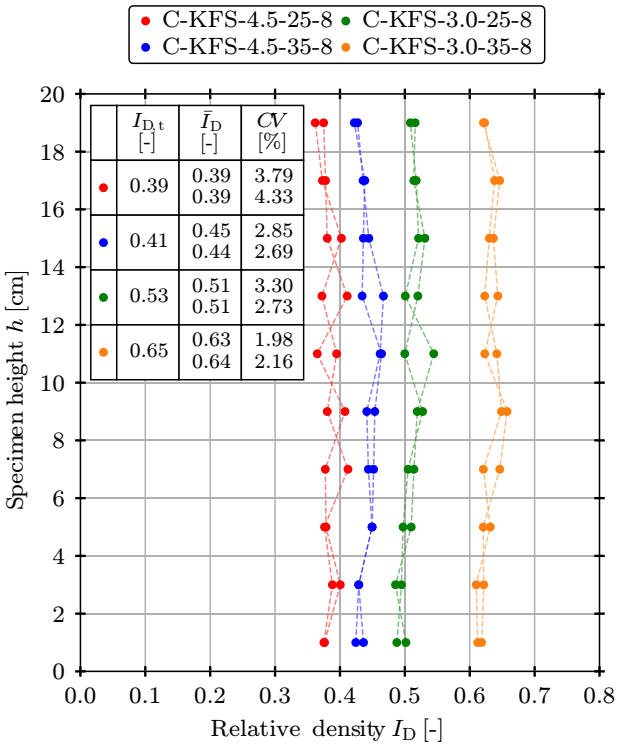

Fig. 21 Relative density distribution in RASP-made KFS-specimens with varying fall height and nozzle diameter

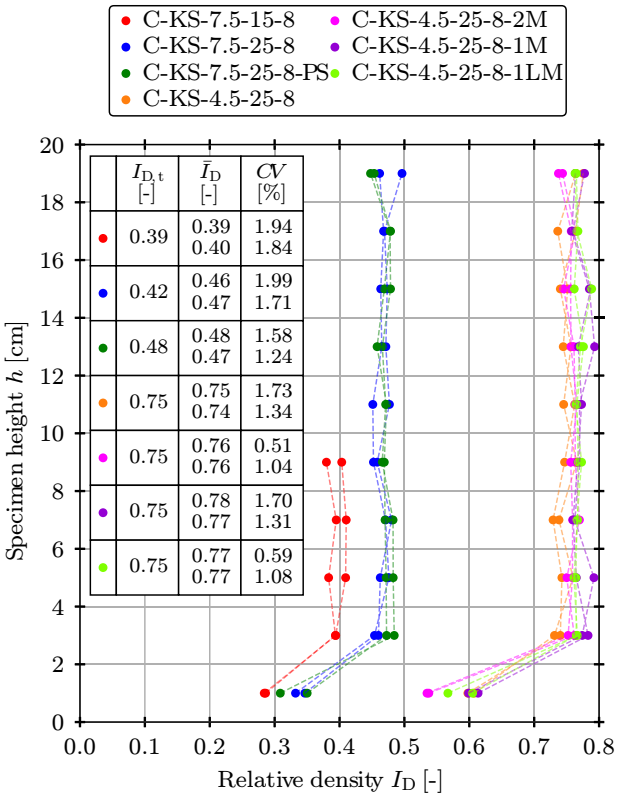

Fig. 22 Relative density distribution in RASP-made KS-specimens with and without membranes above the base plate and with and without lubrication

3.5 Influence of the base plate

All previous tests using KS, irrespective of whether human or RASP-made, show a decreased local density in a bottom layer (bottom PVC ring) of the specimen (Figure 8, Figure 9, Figure 17, Figure 18, Figure 19, Figure 20).

However, the tests using the much finer KFS do not show this base plate effect (Figure 21), which obviously occurs due to the interaction between the falling grains and the base plate. Vaid and Negussey [22] have already shown that, under otherwise identical conditions, the velocity of a smaller grain (with smaller mass) in a free fall through air is lower than the velocity of a larger grain. The impact of KS on the base plate is therefore significantly greater than the impact of the KFS for otherwise constant parameters. It should be noted that kinetic energy scales quadratically with velocity.

Throughout the KS-specimen preparation process for the first layers, it could be observed that the sand stream is not dampened when it hits the PVC base plate and that the individual sand grains therefore bounce around in the mold wildly. These chaotic circumstances loosen the resulting specimen locally. After a sufficiently thick sand layer has already been placed into the mold, the impact of the falling grains is dampened, causing a compaction of the underlying grains.

This base plate effect, which is obviously more pronounced for coarser material, in the preparation of specimens using dry air pluviation from a single nozzle can thus be demonstrated for the first time in this study. In specimens produced by hand, this loose layer may be overshadowed by the general fluctuations, but it still exists (Figure 8). It is noteworthy that, as a result, a large number of soil mechanics tests are likely to be carried out on specimens that are significantly looser near the bottom than above.

In real triaxial tests, however, the base plate is usually made of stainless steel with a small or large porous stone. The base plate can furthermore be covered with one or two membranes and greased for lubrication. To check whether these factors prevent the appearance of the looser soil layer, specimens are produced with and without membranes above the base plate and with or without lubrication (one membrane (1 M), two membranes (2 M), lubrication between one membrane and the base plate (1LM)). In addition, a large porous stone (PS) is placed on the base plate in one test. The measured density distributions are shown in Figure 22.

It can be seen that the examined specifications of the base PVC plate do not erase the aforementioned base plate effect, and the density in the lowest ring is still significantly

Table 3 Statistical summary of RASP and human specimens: mean, minimum, maximum, standard deviation, and 95% confidence interval of the coefficient of variation CV

Method	n [-]	$\bar{CV}$ [%]	max CV [%]	min CV [%]	s_{CV} [%]	95% confidence interval [% ; %]
RASP	80	1.81	4.33	0.51	0.82	[0.21 ; 3.41]
Human total	16	7.35	17.40	2.43	5.27	[0.05 ; 14.65]
Expert	4	4.22	5.52	3.20	–	–
Intermediate	4	3.39	5.43	2.43	–	–
Newbie	8	10.89	17.40	3.45	–	–

smaller than the density in the rings above. The grains are not dampened by the membrane and/or lubrication or the porous stone. In fact, it appears that two membranes without lubrication actually exacerbate the base plate effect, which can be interpreted as the grains hitting the bottom of the mold more elastically. The base plate effect for KS could therefore not be eliminated by any practical experimental method.

In another attempt (not shown), the bottom ring was filled with sand of the target density before the actual specimen preparation, so that the first grains falling from the nozzle landed on a layer of sand that was already two centimeters thick. However, this caused two issues: On the one hand, the energy input of the impacting grains leads to a compaction of this first layer, so that at the end of the specimen preparation, the lower layer is denser than the sand above it. This could be prevented by initially filling the sand more loosely with a iteratively found density. On the other hand, this layer cannot be simply pluviated and must be compacted by vibration or tamping, which induces a significantly different anisotropic microstructure (fabric) than the sand above it.

The base plate effect for the KS specimens tends to increase slightly as the overall density of the specimen increases, regardless of how this higher density is achieved. Greater density can be achieved, for example, by increasing the fall height or reducing the nozzle diameter, which, according to [11, 22], leads to a higher grain velocity and thus a greater impact of the falling grains. Figure 18 has already shown this observation for tests with different nozzle diameters.

To verify the hypothesis that the bottom effect is more pronounced if the overall density of the specimen increases, tests are shown in Figure 22 with different nozzle diameters ($d_\mathrm{n} = 4.5$ mm and $d_\mathrm{n} = 7.5$ mm). To create an even looser specimen, in addition to the tests with a fall height of $h_\mathrm{f} = 25$ cm, a test with a smaller fall height of $h_\mathrm{f} = 15$ cm is performed. However, with the selected fall height of $h_\mathrm{f} = 15$ cm, only the first five rings (specimen height of $H = 10$ cm) could be used so that $H < h_\mathrm{f}$ applies. These tests reveal that the base plate effect is for dense specimens slightly more pronounced than for loose ones. However, the base plate effect is also clearly noticeable for looser specimens.

The observation of the base plate effect poses a significant issue for specimen preparation. It must be concluded that the dry air pluviation technique out of a single nozzle should be interpreted and used with care for coarse materials because an inhomogeneous density distribution due to the base plate effect has to be expected, especially for small specimen heights. It has to be highlighted that this issue arises for both RASP prepared and manually prepared specimens. It was not possible to find any practical methods to prevent this effect. Rotating the specimen and removing the affected layer after production would eliminate this loose area, of course. However, it is likely that rotating the specimen would cause some disturbance. These effects need to be studied in detail in the future.

Finally, it should be noted that the RASP method presented in this paper and the relative densities achieved are highly sensitive to the granular material used. Even minor variations, for example due to a different homogenisation of the specimen material, can require the method to be recalibrated and the cobot parameters to be adjusted.

3.6 Statistical evaluation

In the following, the results shown above are summarized and statistically evaluated together with additional test results not shown in detail above. For this analysis, 80 specimens prepared using the automated RASP method (excluding specimens without a constant value of h_f) and 16 manually prepared specimens (4 by the expert, 4 by the intermediate, and 8 by the newbie) are considered. For each specimen, the coefficient of variation CV is determined based on 8 density measurements, excluding the upper and lower ring. This results in a total of 768 density measurements that are included in the following statistical evaluation.

Table 3 presents the mean value $\bar{CV}$, the corresponding minimum (min CV) and maximum (max CV) values, the standard deviation s_{CV}, and the 95% confidence interval of the coefficient of variation CV for all considered specimens prepared manually and with the RASP. s_{CV} is determined using the CV values of the considered specimens. The 95%

confidence interval also applies to the CV values of the individual specimens.

The coefficient of variation CV, defined in Equation 7, measures density homogeneity within a specimen. CV is normalized by the mean relative density to allow a comparison between specimens with different densities, with lower values indicating higher homogeneity. Furthermore, low CV values can indicate higher reproducibility between different specimens. The results show that specimens produced using the automated RASP method exhibit a significantly lower mean coefficient of variation ($\bar{CV} = 1.81$ %) compared to manually prepared specimens ($\bar{CV} = 7.35$ %), indicating a substantially higher homogeneity and reproducibility of the RASP specimen preparation process.

In addition to the mean values, the standard deviation s_{CV} and the corresponding 95% confidence intervals provide further insight into the variability and statistical robustness of the different preparation methods. RASP specimens show a low standard deviation ($s_{CV} = 0.82$ %) and a comparatively narrow confidence interval of CV, indicating a stable and well-controlled preparation process that yields reproducibly homogeneous specimens. In contrast, manually prepared specimens exhibit a significantly larger standard deviation ($s_{CV} = 5.27$ %) and a very wide confidence interval, reflecting pronounced variability in the manual specimen preparation process. The standard deviation and confidence interval are considered collectively for the manual specimens, as dividing them into individual operators would result in a small number of specimens.

The minimum and maximum achieved CV values further support these observations. RASP specimens cover a narrow range of CV values from 0.51 % to 4.33 %, demonstrating consistent density homogeneity and low sensitivity to process variability. Manually prepared specimens, however, span over a much wider range from 2.43 % to 17.40 %, indicating a considerable risk of producing strongly inhomogeneous specimens when relying on manual preparation.

Among the manually prepared specimens, noticeable differences between the operator groups are observed. Expert and intermediate operators achieve relatively low mean CV values of $\bar{CV} = 4.22$ % and $\bar{CV} = 3.39$ %, respectively, with moderate spreads between minimum and maximum values. Specimens prepared by the newbie, however, show a markedly higher mean coefficient of variation ($\bar{CV} = 10.89$ %) and the largest spread, with CV values ranging from 3.45 % to 17.40 %. This clearly highlights the strong influence of operator experience on the homogeneity of manually prepared sand specimens. Although experience can improve specimen quality, manual preparation inherently lacks the reproducibility and reliability of the automated RASP method.

4 Conclusion

This paper introduces a fully Robotic Automated Specimen Preparation (RASP) method for the dry air pluviation technique for granular material. The proposed device consists of a conventional collaborative six-axis robot (cobot) and a single nozzle installed at the tool end of the robotic arm. The specimen preparation follows a well-defined procedure and is fully automated. The method can be transferred to other robotic systems in a straightforward procedure. The RASP introduced is used to produce overall more than 80 cylindrical specimens with a height of $H = 20$ cm and a diameter of $D = 10$ cm. The local vertical density distribution of the specimen is then determined.

Comparison with human-made specimens reveals that the RASP process leads to significantly more homogeneous and reproducible specimens in terms of the density distribution. In detail, the local density measurements on the RASP specimens show an average coefficient of variation of $\bar{CV} = 1.81$ %, while the ones prepared by hand show a much higher coefficient of variation of $\bar{CV} = 7.35$ %.

Based on this fundamental observation, the effects of the nozzle diameter and the fall height on the achievable density, which are known from the literature, become apparent. It is also proven that the RASP method presented is very robust in itself. The nozzle velocity and pluviation pattern have a practically negligible influence on the resulting density. The proposed method has been confirmed for two different types of sand. RASP additionally provides a detailed documentation of the specimens' preparation process due to the produced data. Especially for large and dense specimens, the RASP method is expected to save laboratory technicians a significant amount of time and effort, and thus financial costs for high-quality geotechnical soil analyses.

However, it is further shown that using the dry air pluviation preparation method with coarse sands, regardless of whether manual or RASP, a looser soil layer at the bottom of the specimen is to be expected. The observation of this base plate effect contradicts the common assumption of a so-called element test.

In the near future, the automatically generated specimens will be tested in conventional soil mechanical experiments (triaxial test, oedometric test), and the variations in the results will be compared against manually prepared specimens. The work presented provokes justified optimism that there will be more consistent and reproducible results in these tests using the RASP method.

Acknowledgements The authors are grateful to Schneider Electric GmbH, namely M. Kimpel, M. Voegele, M. Fleckenstein, and S. Winkler, for their support in commissioning the cobot. We would like to thank F. O. Abimaje for her assistance in taking the photos.

Funding Open Access funding enabled and organized by Projekt DEAL.

Data Availability The data supporting the findings of this study are available from the corresponding author upon reasonable request.

Declarations

Conflict of interest The authors declare that they have no known competing financial interests or personal relationships that could have appeared to influence the work reported in this paper.

References

1. Al-salih O, Al-abboodi I (2023) Assessment of a new pluviation system designed to prepare uniform samples of sand. J King Saud Univ- Eng Sci 38(3):24
2. Anilkumar R, Martinez A (2025) Experimental investigation of circumnutation-inspired penetration in sand. Bioinspiration & Biomimetics 20(1):016006
3. Beverloo WA, Leniger HA, van de Velde J (1961) The flow of granular solids through orifices. Chem Eng Sci 15(3):260–269
4. Bi ZM, Luo C, Miao Z, Zhang B, Zhang WJ, Wang L (2021) Safety assurance mechanisms of collaborative robotic systems in manufacturing. Robot Comput-Integr Manuf 67:102022
5. Chen Y, Yang J (2024) Small-strain shear modulus of silty sands: the role of sample preparation method. Géotechnique 74(4):367–382
6. Della N, Arab A, Belkhatir M (2011) Influence of specimen-reconstituting method on the undrained response of loose granular soil under static loading. Acta Mech Sin 27(5):796–802
7. Jin Z, Shi Z, Hambleton JP (2020) Small-scale Geotechnical Testing Using a Six-axis Robot. Technical Report 20-7/495S
8. Knittel L, Lamparter A, Niemunis A, Stutz HH (2023) The high-cyclic model for sand tested beyond the usual ranges of application. Acta Geotechnica, pages 1–12
9. Ladd RS (1974) Specimen preparation and liquefaction of sands. J Geotech Eng Div ASCE 100(GT10):1180–1184
10. Ladd RS (1978) Preparing test specimens using undercompaction. Geotech Test J ASTM 1(1):16–23
11. Lagioia R, Sanzeni A, Colleselli F (2006) Air, Water and Vacuum Pluviation of Sand Specimens for the Triaxial Apparatus. Soils Found 46(1):61–67
12. Li XS, Dafalias YF (2012) Anisotropic critical state theory: role of fabric. J Eng Mech 138(3):263–275
13. Mankoc C, Janda A, Arévalo R, Pastor JM, Zuriguel I, Garcimartín A, Maza D (2007) The flow rate of granular materials through an orifice. Granular Matter 9(6):407–414
14. Miura S, Toki S (1982) A sample preparation method and its effect on static and cyclic deformation-strength properties of sand. Soils Found 22(1):61–77
15. Miura S, Toki S (1984) Anisotropy in mechanical properties and its simulation of sands sampled from natural deposits. Soils Found 24(3):69–84
16. Mugele L, Stutz HH, Yang ZX (2025) Accounting for cyclic and fabric effects in an enhanced hypoplastic model for sand. Comput Geotech 187:107462
17. Mugele L, Zürn J, Niemunis A, Stutz HH (2025) Experimental study of the soil structure variable z used in constitutive models such as Neohypoplasticity or Sanisand. IOP Conf Ser Earth Environ Sci 1480(1):012070
18. Oda M (1972) Initial fabrics and their relations to mechanical properties of granular material. Soils Found 12(1):17–36
19. Passalacqua R (1991) A sand-spreader used for the reconstitution of granular soil models. Soils Found 31(2):175–180
20. Schröder S, Biele J, Block J, Roll R, Ulamec S, Witte L (2013) Philae Landing Test at the Landing and Mobility Test Facility (LAMA)
21. Tatsuoka F, Ochi K, Fujii S, Okamoto M (1986) Cyclic undrained triaxial and torsional shear strength of sands for different sample preparation methods. Soils Found 26(3):23–41
22. Vaid YP, Negussey D (1984) Relative density of pluviated sand samples. Soils Found 24(2):101–105
23. Vogelsang J (2017) Untersuchungen zu den Mechanismen der Pfahlrammung. Dissertation, Karlsruhe Institute of Technology, Institute for Soil Mechanics and Rock Mechanics, Issue 182, Karlsruhe,
24. Vogelsang J, Huber G, Triantafyllidis T (2017) Experimental Investigation of Vibratory Pile Driving in Saturated Sand. In: Triantafyllidis T (ed) Holistic Simulation of Geotechnical Installation Processes. Springer, Cham, pp 101–123
25. Wichtmann T (2016) Soil behaviour under cyclic loading - experimental observations, constitutive description and applications. Habilitation, Karlsruhe Institute of Technology, Institute for Soil Mechanics and Rock Mechanics, Issue 181, Karlsruhe
26. Wichtmann T, Steller K, Triantafyllidis T (2020) On the influence of the sample preparation method on strain accumulation in sand under high-cyclic loading. Soil Dyn Earthq Eng 131:106028
27. Wichtmann T, Triantafyllidis T (2016) An experimental database for the development, calibration and verification of constitutive models for sand with focus to cyclic loading: part I-tests with monotonic loading and stress cycles. Acta Geotech 11(4):739–761
28. Yang ZX, Li XS, Yang J (2008) Quantifying and modelling fabric anisotropy of granular soils. Géotechnique 58(4):237–248
29. Zuriguel I, Garcimartín A, Maza D, Pugnaloni LA, Pastor JM (2005) Jamming during the discharge of granular matter from a silo. Phys Rev E 71(5):051303
30. Zürn J, Mugele L, Stutz HH (2024) Novel experimental method for rate-independent triaxial tests under partial drainage condition. Géotechnique Letters 14(3):100–105